



Earthquake Building Damage Detection Using VHR Satellite Data (Case Study: Two Villages Near Sarpol-e Zahab)

Babak Mansouri^{1*}, Shakiba Mousavi², and Kambod Amini-Hosseini¹

1. Associate Professor, Earthquake Risk Management Research Center, International Institute of Earthquake Engineering and Seismology (IIEES), Tehran, Iran,

* Corresponding Author; email: mansouri@iiees.ac.ir

2. Ph.D. Student, International Institute of Earthquake Engineering and Seismology (IIEES), Tehran, Iran

Received: 29/07/2018

Accepted: 29/08/2018

ABSTRACT

A strong earthquake with Mw 7.3 occurred on Nov. 12, 2017, at the Iran-Iraq border where the city of Sarpol-e Zahab (24 km from the epicenter) and many other towns and villages were affected severely. Rapid damage mapping essentially helps to understand the location, the extent and the severity of high hit areas, and it is regarded as an important source of information in assisting proper crisis management. Rapid damage mapping can be completed according to three general methods namely; manual, semi-automated, and automated. This research explores a proposed semi-automated method that once calibrated and operational it can be utilized as an automated process. After preprocessing the satellite data, individual buildings or building parcels are identified using either some building extraction tools or with the use of some ancillary data sets. The proposed damage detection algorithm is based on deriving a set of textural indices associated to individual building or property footprints. These parameters have been input into an Artificial Neural Network (ANN) for damage classification. The trained ANN created urban damage maps. For detecting significant observable physical changes/damages to the buildings, two schemes were developed: 1) by comparing the post-event with the pre-event VHR satellite images, and 2) using a post-event image only. In scheme-1, before and after images were acquired from different satellites (TripleSat_2 with 89 cm and SVI with 50 cm spatial resolution) as input and the Overall Accuracy (OA) of the proposed damage classification was reported as 72%. The damage classification accuracy in scheme-2 produced an OA of 75%.

Keywords:

Object-oriented image processing; Damage detection; Textural analysis; Artificial Neural Network

1. Introduction

Natural disasters such as devastating earthquakes are affecting lives of millions of people around the world each year. Large earthquakes are unpredictable and rare with high consequences when occurring in urban or rural settings. The buildings are amongst the most important urban elements since they provide shelters and at the same time threat the lives of its occupants. For such disastrous

events, damage mapping is inevitable for effective disaster mitigation and management.

There are several practical methods to generate change maps. Direct visual observation is one of the methods but suffers from low speed for data collection and limited access to all damaged areas given the allocated resources. Alternatively, remote sensing technology can be considered as a useful

tool in collecting information faster with adequate accuracy. High resolution data such as satellite/aerial imageries can be efficient to prepare change/damage maps. The spatial resolution of such data sets needs to be high enough to be able to discriminate between objects such as buildings and other features. Change maps can be derived utilizing the following methods:

1. Comparison of pre and post images from the same sensors (multi-temporal);
2. Comparison of pre and post images from different sensors (multi-temporal and multi-sensor);
3. Damage inferencing utilizing a single post-event image (mono-temporal).

In recent years, accurate, fast and efficient automated pixel-based and object-oriented methods have been developed and proposed in deriving geometrical or textural changes from satellite images. Besides, damage detection algorithms were proved to be effective in estimating earthquake damages in urban areas. Gamba and Casciati [1] developed a rapid damage detection algorithm for building damage assessment using pre- and near-real-time post-event aerial images. This method is based on shape analysis and perceptual grouping. Comparing the outcome of this method with the results of visual interpretation, about 70% of the collapsed buildings could be detected correctly.

There is a general tendency that visually interpreted damage survey using satellite images underestimate physical damages [2]. Yamazaki et al. [3] visually estimated damages from Quickbird images and determined different damage grades according to the EMS-98 procedure. In order to assess the accuracy, field data collected by Hisada et al. [4] was utilized. The comparison revealed that the best accuracy was achieved for the completely damaged buildings (EMS-98, Grade 5) and for the slightly and moderate damaged buildings (EMS-98, Grade 1 and 2).

Gusella et al. [5] provided an object-oriented methodology using eCognition image processing software [6] to carry out damage detection by supervised method identifying 'collapsed' versus 'no-collapsed' buildings. The reported Producer Accuracy (PA) was 67.4% for 'collapsed' and 74.4% for 'no-collapsed' cases. Moreover, the User Accuracy (UA) was 78.5% for 'collapsed' and 62.5%

for 'no-collapsed' buildings.

Mansouri et al. [7], using pre- and post- VHR data of Bam earthquake in tandem with buildings inventory data sets and applying a fuzzy logic algorithm were able to determine the extent and the severity of building destruction caused by the 2003 earthquake in Bam. Comparing these results with an observed damage map revealed an agreement of 72% for severe building damaged category. Mansouri and Hamednia [8] used a soft computing methods combining GA (Genetic Algorithm) and SVM (Support Vector Machine) in order to select optimum feature sets for damage mapping using VHR optical satellite imagery for the 2003 Bam earthquake. The proposed algorithm was evaluated by comparing the produced damage map with a reference data as ground truth showing overall accuracies of 76% for detecting three levels of structural damage (i.e. no to slight, moderate, and heavy to destruction) and 89% for determining binary damage levels as no-collapse, and collapse. Mostafazadeh and Mansouri [9] presented a semi-automated building extraction and damage detection algorithms employing Haralick features and Artificial Neural Network (ANN) classification tools. Building extraction showed an overall accuracy of 91% where compared with an existing urban database. The damage was classified according to an optimal feature set. The overall accuracy for damage mapping using an optimal second order Haralick feature set was reported as 73%.

2. Study Area - Earthquake Damages

On November 12, 2017 at 9:48 pm local time a strong earthquake with Mw 7.3 occurred on the Iran-Iraq border. In this event, the province of Kermanshah was the most affected area with the city of Sarpol-e Zahab being the hardest-hit zone. According to a recent report, about 518 out of a total of 579 people were killed in Sarpol-e Zahab and thousands more were injured. The earthquake caused serious damages in structures in a wide area in the state of Kermanshah, most of which were rural. In Sarpol-e Zahab, the widespread destruction on poor quality constructions were reported and many recently buildings were collapsed while older buildings were practically intact. The north-west



Figure 1. Post-event Google Earth image of study area Ghara-Belagh-Azam and Shahrak Zeraee [10].

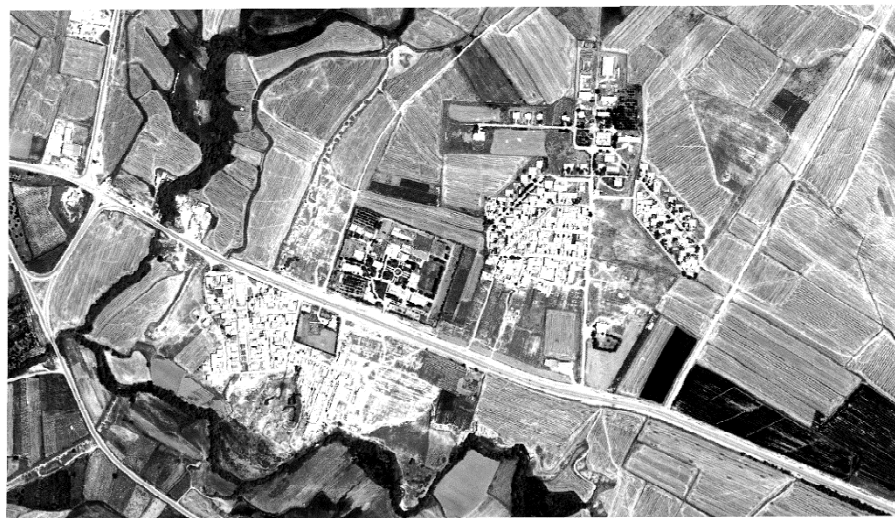


Figure 2. Pre-event panchromatic image of study area (courtesy of TRIPLESAT_2).

area comprised of rather newly built dwellings but without proper earthquake resistance. The southern band of the city contained vulnerable older buildings. Both these areas suffered devastating damages and casualties. Two highly hit villages namely Ghara-Belagh-Azam and Shahrak Zeraee adjacent to the northwest of the city were selected for this study. For this area, a reconnaissance trip has been conducted by the authors where the extent and the general aspects of building damages were observed. The dominant construction types were recognized as low-rise poor masonry or weak steel structures with infill brick walls, **Figure (1)**.

3. Imagery, Building Data, Ground Truth

In this study, Chinese TRIPLESAT_2 and SV1

satellites were acquired for both before and after the event. The specifications of these satellites are listed in Table (1). TripleSat_2 is a constellation of three identical Beijing-2 satellites. SV1 or SuperView1 is among the latest China high-resolution optical commercial satellites. Parts of the satellite images for both pre-EQ and post-EQ showing the study area are presented in Figures (2) and (3).

Table 1. Satellite data general specification.

Satellite	Spatial Resolution		Acquisition Date
	PAN (m)	MS (m)	
TRIPLESAT_2	0.89	3.2	Pre-Event: 2016-06-04
SV1	0.5	2	Post Event: 2017-11-16



Figure 3. Post-event panchromatic image of study area (courtesy of SV1).



Figure 4. Aerial photography for high hit zones (courtesy of IRIB news agencies).

The pre-event image quality was not as adequate as the post-event image. It was not efficient to apply the automated segmentation algorithm (e.g. using the eCognition software) in order to extract building objects. Such algorithm is based on region-merging technique and when using poor resolution data, it confuses between adjacent blurred objects. Therefore, for object-based image analysis, a building mask map was utilized for extracting textural contents from all building footprints from these two images. This building mask has been created by complementing the Open Street Map data containing most of the parcel polygons with manually drawing the missing buildings on Google Earth images. All these data were unified within a GIS application. According to the reconnaissance and observing the imageries for the disaster zones (Figures 3 and 4), signatures of vertical collapse (pancake) and debris hips generated from exterior walls of the buildings were revealed. To cover

almost all possible building-related damages, the "building objects" have been actually taken as the "property mask" comprised of the building footprints and the associated yards (lands) as shown in Figure (5).



Figure 5. Building mask defined as individual property boundaries (building footprint and yard).

Since the ground truth information and the survey data of the study area was not available, visual interpretation of post-earthquake satellite image was performed as a reference damage map for evaluating the building damage detection accuracy. One way for creating a reference damage map is by visual interpretation of severely damaged or collapsed buildings by comparing pre- and post-satellite imageries. Usually lower damage grades are difficult to identify, so the pre-event imagery can be helpful in detecting such minute changes through visual interpretation. In this study, only post-event image has been used for visual ground truth due to its better available spatial resolution. For better visualization and manual damage mapping, pansharpened post-event Pleiades-1A has been utilized where the data specification is listed in Table (2). The final reference damage map shown in Figure (6) was produced by inferring the severity of changes and the signatures of the debris within and around the building footprints (modifying and completing the Iranian Space Agency damage map). According to this satellite-

based damage mapping, the building pool was classified into two classes of "Changed/Collapse" or "Unchanged/No Collapsed". Change/damage patterns for the building footprints are explained in Table (3) where building damage classification are interpreted visually from post-earthquake satellite image.

Table 3. Building damage classification according to visual interpretation from post-earthquake satellite image.


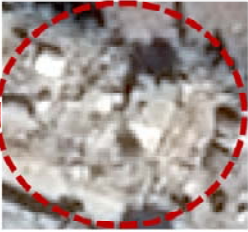
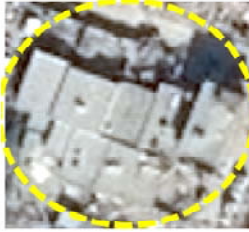
Building Footprints as Seen from Satellite Images	
	
Pattern Classification with Visual Interpretation	
Changed (Collapsed) Buildings Shown in Red	Unchanged (No Collapsed) Buildings Shown in Yellow
	

Table 2. Specification of Pleiades-1A used for damage map referencing.

Satellite	Spatial Resolution		Acquisition Date	Satellite Operator
	PAN (m)	MS (m)		
Pleiades-1A	0.5	2	16 Nov 2017	Planet Lab, USA



Figure 6. Reference damage map according to the visual interpretation of post-earthquake satellite image.

4. Damage Mapping Methodology

The purpose of this study is to present an object-oriented semi-automated method for city-wide damage mapping. Preprocessing the pre-event and post-event images included geo-referencing and matching the images together. In this method, all image analysis and related computations were performed for the extracted individual property (both building and yard) masks. In order to delineate effectively between "changed" or "unchanged" areas, GLCM (Grey Level Co-occurrence Matrix) Haralick textural images were created. Haralick et al. [11] suggested 14 different measures computable in four main directions. The Grey Level Co-occurrence Matrix (GLCM) represents not only the relationship between the brightness values of adjacent pixels, but also reveals how often distinct combinations of grey levels occur in an image. Textural index extraction from GLCM exhibits second-order histogram statistics where pixel relationships are taken into account. The textural relative difference of temporal images were produced for the textural features as listed in Table (4). Two schemes were used for damage mapping. In the first scheme, not only seven Haralick textural features but also the statistical correlation was computed for each individual building objects (property parcels) as applied to the before and after image pairs. This statistical

correlation in addition to the mentioned textural indices were considered as input to the proposed artificial neural network where two classes of "changed" and "unchanged" are specified. In the second method, only the post-event image has been taken into account. This is because in many instances "before" data cannot be accessible for comparison or there is a spatial resolution incompatibility between before and after images. For this, seven Haralick textural indices were computed for the building objects in the post image, and finally the ANN has been trained according to the reference data in order to produce the city-wide damage map. Figure (7) depicts the flowchart describing the steps involved in both schemes for the presented methodology.

4.1. Pre-processing

Preprocessing the pre-event and post-event images included geo-referencing and matching the images together. This include all satellite images whether for before or after the event and also the ancillary data as building parcel layer. It should be also noted that the spatial resolution for some of the satellite imageries differed from each other; therefore, one must match and scale the image accordingly. In this study, TripleSat-2 had a resolution of 0.89 m, but SV1 showed a much better resolution of 0.5 m.

Table 4. Haralick textural features (as utilized) from GLCM matrix.

Feature	Formula	Description
Mean	$\frac{1}{2} \sum_i^M \sum_j^M (iP[i,j] + jP[i,j])$	Co-occurrence mean value
Variance	$\frac{1}{2} \sum_i^M \sum_j^M ((i - \mu)^2 P[i,j] + (j - \mu)^2 P[i,j])$	Measure of heterogeneity – strongly correlated to first order statistical variable such as standard deviation. Variance increases when gray level variation is high in the kernel.
Homogeneity	$\sum_i^M \sum_j^M \frac{P[i,j]}{1 + i - j }$	Homogeneity measures the similarity of pixels. A diagonal gray level co-occurrence matrix gives homogeneity of 1. It becomes large if local textures only have minimal changes.
Contrast	$\sum_i^M \sum_j^M (i - j)^2 P[i,j]$	Indicates the amount of local variation in an image. Values on the GLCM diagonal show no contrast and increases away from the diagonal in the kernel.
Dissimilarity	$\sum_i^M \sum_j^M i - j P[i,j]$	Similar to contrast but increases linearly. If contrast of area is high, dissimilarity is also high.
Second Moment	$\sum_i^M \sum_j^M P[i,j]^2$	Uniformity or Energy – shows textural uniformity in the kernel. It is 1 when variation in the spectral responses are
Entropy	$-\sum_i^M \sum_j^M P[i,j] \log P[i,j]$	A measure of randomness. Entropy is large when the image is not texturally uniform and many GLCM elements have very small values. Entropy is strongly, but inversely correlated to energy.

$P[i, j]$: Co-occurrence probability of pixel pairs with i and j

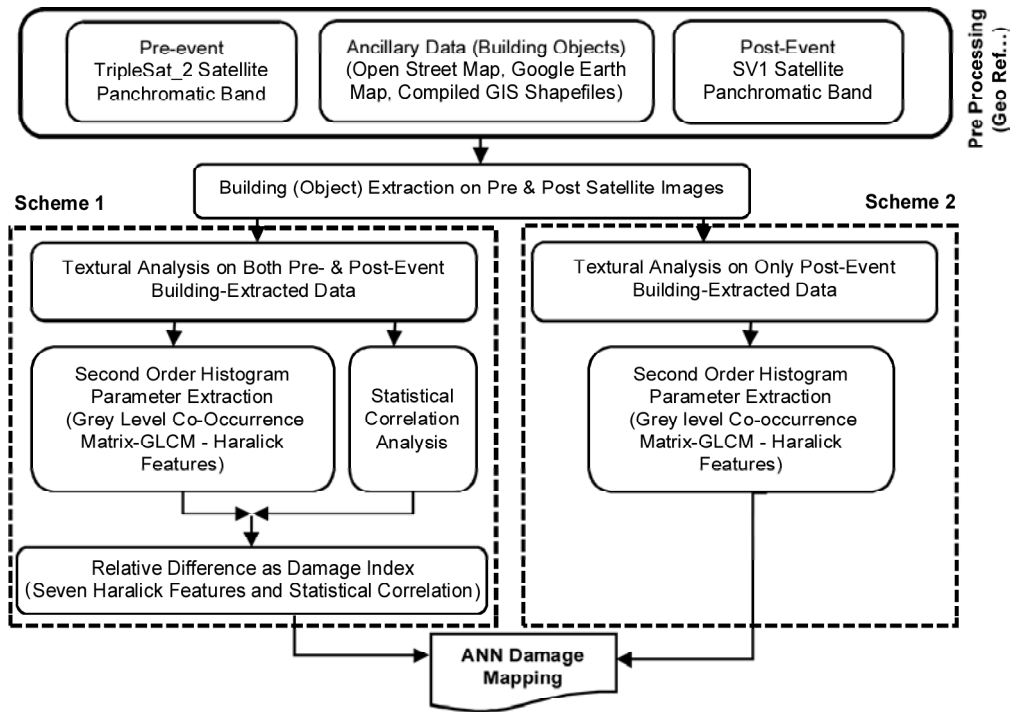


Figure 7. Flowchart of the proposed method.

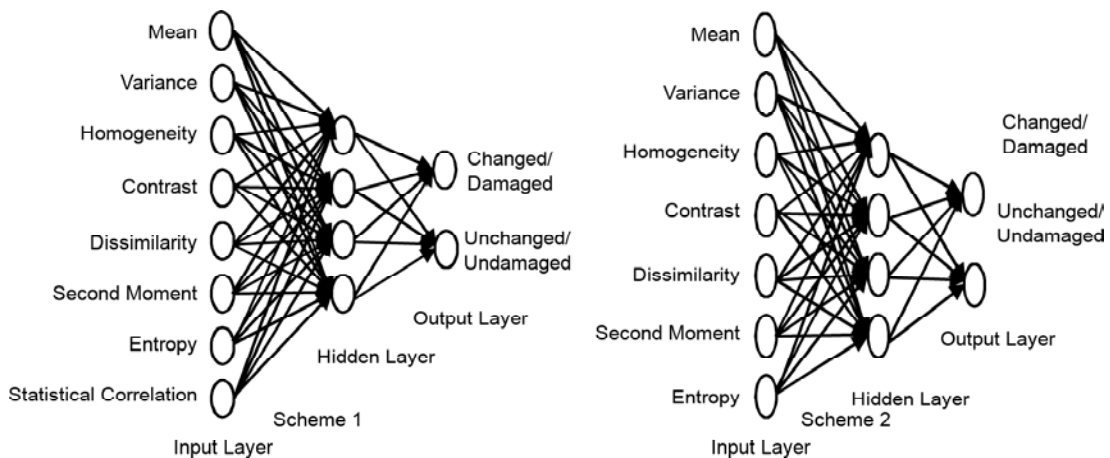


Figure 8. Proposed ANN structure for change/damage detection.

4.2. Textural Feature Extraction

Generally, the destroyed buildings tend to have a coarser textural signature and less gray scale level. Textural analysis is sought as it is suitable for detecting differences between changed and unchanged areas for determining the physical damages to the buildings. The GLCM indicates the prevalence of co-occurrence between different pixel values as similar to a joint probability concept. The second order statistics of an image can be obtained from GLCM, which accounts for the spatial inter-dependency or co-occurrence of two pixels at specific relative positions. In this study, seven Haralick measures were used to extract useful texture

information from pre and post images. These seven features are described briefly in Table (4).

4.3. Artificial Neural Networks Damage Mapping

Soft computing ANN is regarded as an effective technique for classification or decision problems. The neural network has many advantages and capabilities such as adaptive learning, generalization, and classification. ANN is usually very systematic and straightforward to implement. In that, the system learns from some train data sets and then sets itself up for systematically classifying the whole entries in an automated fashion. Figure (8) depicts the ANN feed-forward architecture as implemented

in this study where the number of separated input indices are eight for the scheme one, and seven for scheme two, each having a hidden layer of four nodes and an output layer of two nodes indicating two distinct levels of changed (collapsed) and unchanged (no collapsed). A sigmoid transfer function has been used for the activation of the neurons. The above ANN architecture and the associated algorithm were implemented using the Neural Network Toolbox of Matlab computer code.

5. Implementation and Results

In this study, the panchromatic bands of TripleSat_2 as pre-EQ image and SV1 as post-EQ satellite image were used. After pre-processing, all pixels concerning individual building objects have been extracted from pre-event and post-event satellite images using the building mask. Then, Haralick textural features were extracted for all pre and post images. All Haralick textural features mentioned in Table (4) were computed according to a co-occurrence shift of 1 with a processing window of 3 pixels by 3 pixels. Moreover, these values were averaged along the 0° , 45° , 90° , and 135° .

Scheme 1: Both pre-event and post-event data were utilized and the damage detection algorithm tends to reflect within object changes. The input change indices are set as the relative differences (from pre_ and post_ data) of the seven textural features per individual building objects. In addition to the seven Haralick features, the statistical correlation values have been also computed for each individual objects (building property layout) considering both before and after satellite images having in mind that a higher values would reflect no detectable changes and vice versa.

Scheme 2: Only post-event data has been utilized; therefore, the change indices are considered as the pure Haralick features and the comparison in between different objects has been sought.

Potentially and intuitively, the first scheme is able to provide better/higher damage classification accuracy when using high quality RS data with similar high spatial resolution as compared with the case of second scheme when only one after image is utilized (with the same spatial resolution). However, in this study, since different VHR satellite

images with different spatial resolution and various image qualities were used, the classification results were investigated for both schemes.

ANN Results: A total of 130 buildings were chosen randomly as train data set from the reference ground truth data where about half of them indicated "changed" and the other half referred to "unchanged". Thereafter, the trained ANN was employed for creating the entire damage map of the region. To assess the accuracy of the classification, the confusion matrix has been created based on the reference data and the model result. As seen in Figures (9) and (10), red polygons show detected drastic changes and green polygons represent non-detectable changes. The confusion (or error) matrix is a useful tool for assessing the accuracy of a proposed classification method. In this study, the results obtained from the manual process (as ground truth) are compared with the outcome of the ANN algorithm. The Overall Accuracy (OA) is the percentage of the objects (individual houses) that are correctly classified in the confusion matrix. The Producer's Accuracy (PA) shows the probability of a reference data set (ground truth) being correctly classified by the classifier algorithm. This is the percentage of the number of correctly classified objects in each class from the total number of objects in that class (derived from the reference samples). The User's Accuracy (UA) expresses the probability that an object on the image represents that class on the ground and is the ratio between the number of correctly classified object in a class and the total number of classified objects in that specific class. ANN's confusion matrix for the classification results are shown in Tables (5) and (6).

The proposed model produces an Overall Accuracy of 72%, a Producer's Accuracy of 60% for "Changed" and 76% for "Unchanged", and a User's Accuracy of 48% for the "Changed" and 84% for the "Unchanged" classes in scheme 1. For scheme 2, the overall accuracy is calculated as 75%. The Producer's Accuracy of 68% for "Changed" and 78% for "Unchanged", and a User's Accuracy of 53% for the "Changed" and 87% for the "Unchanged" classes. These figures show that the algorithm was more effective for detecting the "Unchanged" class.



(a) Damage Mapping for Ghara-Belagh-Azam Using Both Pre_Event and Post_Event Images



(a) Damage Mapping for Ghara-Belagh-Azam Using Only Post_Event Damage Image



(b) Dmage Mapping for Shahrak_Zeraee Using Both Pre_Event and Post_Event Images



(b) Dmage Mapping for Shahrak_Zeraee Using Only Post_Event Damage Image

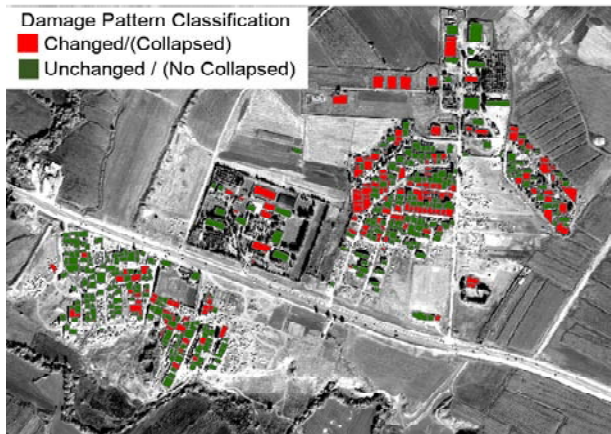


Figure 9. Damage mapping for two villages using both pre event and post event images.

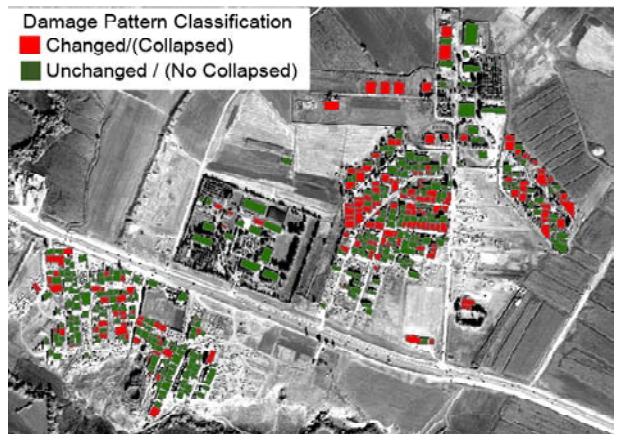


Figure 10. Damage mapping for two villages using only post event damage image.

Table 5. ANN's confusion matrix for pre event and post event images.

Confusion Matrix	Reference Data (Ground Truth)			sum	UA
	Changed/ Collapsed	Unchanged/ No Collapsed			
ANN Classification	76	83	159	0.48	
	50	270	320	0.84	
	126	353		OA = 0.72	
	PA	0.60	0.76		

Table 6. ANN's confusion matrix for only post event damage map.

Confusion Matrix	Reference Data (Ground Truth)			sum	UA
	Changed/ Collapsed	Unchanged/ No Collapsed			
ANN Classification	85	77	162	0.53	
	41	276	317	0.87	
	126	353		OA = 0.75	
	PA	0.68	0.78		

6. Conclusion and Discussion

Rapid damage mapping is sought to understand the location, the extent and the severity of high hit areas as it is regarded as an essential source of reliable information assisting effective crisis management. The proposed rapid damage mapping is based on a semi-automated scheme that once calibrated and operational can be utilized as an automated process for large geographic extents.

The steps involved in this procedure can be summarized as: preprocessing, creating reference dataset for accuracy evaluation, individual building/property object extraction, computation of Haralick texture features and determining damage indices for building parcel objects, ANN setup and training the dedicated artificial neural network and finally damage map production. A rational way to create damage indices is by using both pre and post data. However, because the availability of some before-event satellite images is not guaranteed all the time, using only the post-event data is also focused in this research. The inputs for ANN are all computed damage indices and its output is the classification result reflecting two classes of "changed/collapsed" and "unchanged/no collapsed". The confusion matrix suggests an overall accuracy of 72% when both before and after images were utilized, and 75% for the case where only after image was utilized respectively. The ANN damage mapping from pre-event and post-event data reveal an overall damage ratio of 0.37 for the region. When using solely the post-event data, the overall damage ratio has been calculated as 0.39. One major justification for the fact that both methods resulted in nearly the same values is that the pre-event data (used in the first scheme) although considered as VHR, but suffered from lower spatial resolution (about two times coarser than SV1 data), and poorer quality, and it is believed to have affected the damage index calculation accuracy. Considering the extent of the scenes, the effectiveness of the algorithm and the computational capabilities of regular personal computers, the processing time for scheme-1 is slightly more than for scheme-2 but not practically a determining factor.

Acknowledgement

This research is completed under the International

Institute of Earthquake Engineering and Seismology sponsorship to study the Nov. 12, 2017 Sarpol-e Zahab earthquake. China GEOSS is acknowledged for providing optical VHR images from TRIPLESAT_2 and SV1 satellites for the region under the study free of charge. Post-event Pleiades-1A VHR image and a preliminary damage map was provided by the Iranian Space Agency for this applied research.

Reference

- Gamba, P. and Casciati, F. (1998) GIS and image understanding for near-real-time earthquake damage assessment. *Photogrammetric Engineering and Remote Sensing*, **64**, 987-994.
- Saito, K., Spence, R.J., Going, C., and Markus, M. (2004) Using high-resolution satellite images for post-earthquake building damage assessment: a study following the 26 January 2001 Gujarat earthquake. *Earthquake Spectra*, **20**(1), 145-169.
- Yamazaki, F., Yano, Y., and Matsuoka, M. (2005) Visual damage interpretation of buildings in bam city using quickbird images following the 2003 bam, Iran, earthquake. *Earthquake Spectra*, **21**(S1), 329-336.
- Hisada, Y., Shibayama, A., and Ghayamghamian, M.R. (2005) Building damage and seismic intensity in Bam City from the 2003 Iran, Bam, Earthquake. *Bulletin of Earthquake Research Institute, University of Tokyo*, **79**(3 & 4), 81-94.
- Gusella, L., Adams, B.J., Bitelli, G., Huyck, C.K., and Mognol, A. (2005) Object-oriented image understanding and post-earthquake damage assessment for the 2003 Bam, Iran, earthquake. *Earthquake Spectra*, **21**(S1), 225-238.
- www.ecognition.com.
- Mansouri, B., Shinozuka, M., Huyck, C., and Houshmand, B. (2005) Earthquake-induced change detection in the 2003 Bam, Iran, earthquake by complex analysis using Envisat ASAR data. *Earthquake Spectra*, **21**(S1), 275-284.
- Mansouri, B. and Hamednia, Y. (2015) A soft computing method for damage mapping using

VHR optical satellite imagery. *IEEE Journal of Selected Topics in Applied Earth Observations and Remote Sensing*, **8**(10), 4935-4941.

9. Mostafazadeh, M. and Mansouri, B. (2015) Object-oriented building extraction from VHR satellite data and earthquake damage detection based on textural analysis using artificial neural network. *Bulletin of Earthquake Science and Engineering*, **2**(1), 55-65.
10. <http://www.gosur.com/google-earth>.
11. Haralick, R.M., Shanmugam, K., and Dinstein, I.H. (1973) Textural features for image classification. *IEEE Transactions on Systems, Man and Cybernetics*, **SMC3**(6), 610-621.